

Double Splay Nematic Order in Confined Polar Fluids

Zhongjie Ma¹, Miao Jiang¹, Aile Sun¹, Shengzhu Yi^{1,2}, Jidan Yang³, Mingjun Huang^{3,4}, Satoshi Aya^{3,4}, Qi-Huo Wei^{1,5*}

¹ Department of Mechanical and Energy Engineering, Southern University of Science and Technology, Shenzhen, 518055, China

² Department of physics, The Hongkong University of Science and Technology, Clear Water Bay, Hong Kong, China

³ South China Advanced Institute for Soft Matter Science and Technology (AISMSST), School of Emergent Soft Matter, South China University of Technology, Guangzhou 510640, China

⁴ Guangdong Provincial Key Laboratory of Functional and Intelligent Hybrid Materials and Devices, South China University of Technology, Guangzhou 510640, China

⁵ Center for Complex Flows and Soft Matter Research, Southern University of Science and Technology, Shenzhen 518055, China

In this study, we demonstrate that when a ferroelectric nematic is confined between two glass plates coated with ionic polymers, a modulated phase emerges in a narrow temperature range between the nematic and ferroelectric nematic phases. This modulated phase emerges from the nematic phase in a continuous manner and then transforms into the ferroelectric nematic phase via a first-order transition upon cooling. Using optical microscopy, we provide compelling evidence that this modulated phase corresponds to the theoretically predicted double splay nematic phase. In this phase, splay deformations alternate in two orthogonal directions oriented at 45° to the substrate surfaces, creating a modulation wavelength that is twice the thickness of the cell. Our experiments with different ionic coatings reveal that only polymeric cationic coatings effectively promote the formation of this phase, highlighting the critical role of electrical screening. These findings not only confirm the existence of the double splay nematic phase but also provide insights into the distinctive topological defects of this phase in confined geometries.

Nematic (N) liquid crystals are a state of matter in which anisotropic molecules are positioned randomly while aligned along a common direction known as the director \mathbf{n} . In this phase, the liquid crystal retains inversion symmetry, such that $\mathbf{n} = -\mathbf{n}$ [1]. Ferroelectric nematic (N_F) liquid crystals, which are the polar fluids predicted over a century ago and realized in experiments only in recent years [2-7], consist of rod-shaped molecules with large electric dipoles. The N_F liquid crystals exhibit both orientational ordering and spontaneous electrical polarization \mathbf{P} [5-8]. This spontaneous polarization aligned typically parallel to the director ($\mathbf{P} = P_0 \mathbf{n}$), not only breaks the inversion symmetry but also exerts profound impact on the director fields due to the interplay of flexoelectricity and electrostatic interactions. These effects can lead to non-trivial ground states and topological excitations [9-19].

Flexoelectricity originates from the coupling between polarization and elastic deformations in the director field [20,21]. In the N_F liquid crystals, the molecules are typically pear-shaped, and thus their close packing requires splay deformations [7,22,23]. This arrangement results in a positive flexoelectric coupling coefficient, denoted by λ , and an associated free energy given by $F_{Flexo} = -\lambda \int dr^3 \mathbf{P} \cdot \mathbf{n} \nabla \cdot \mathbf{n}$ [14,24,25]. As a result, the director field tends to adopt some degree of splay deformation. To fill the entire space, the direction of the splay deformation can alternate along one axis, leading to the formation of a single splay nematic (N_S) phase [26,27]. Recent theoretical study by Rosseto and Selinger, dubbed hereafter as RS theory, suggests that a double splay nematic phase, where splay deformations alternate in two orthogonal directions [28], could be more stable than the single splay nematic phase.

Experimental studies have provided evidence for the single splay nematic phase as an intermediate state between the nematic and ferroelectric nematic phases in ferroelectric nematic materials [29,30]. The transition from the nematic phase to the splay nematic phase has been identified as a weakly first-order transition [31,32], characterized by significant pretransitional splay fluctuations and an exothermic peak [29,30]. This modulated splay phase is recognized as biaxial and antiferroelectric, and the $N-N_S$ phase

transition can be seen as an orientational analogue of the ferroelastic transition [29,30], mediated by flexoelectric coupling.

Electrostatic interactions in ferroelectric nematic materials cause an increase in the free energy by: $F_{Elec} = \iint d^3 r_1 d^3 r_2 \rho(\mathbf{r}_1) \rho(\mathbf{r}_2) e^{-r_{12}/\Lambda} / 4\pi r_{12}$, where Λ is the Debye screening length and r_{12} is the distance between the positions \mathbf{r}_1 and \mathbf{r}_2 [24]. The charge density ρ includes both surface and bound charges. Surface charges arise from the tilt of polarization at the confining surfaces, and their density given by: $\rho_S = (\mathbf{P} \cdot \mathbf{v}) \delta(\mathbf{v} \cdot \mathbf{r} - r_{surf})$, where \mathbf{v} is the surface normal vector, and δ is the Dirac delta function with a unit of 1/length and maximum at surfaces [24]. Bound charges, on the other hand, result from splay deformations in the polarization field, with the charge density expressed as: $\rho_B = -\nabla \cdot \mathbf{P} = -P_0 \nabla \cdot \mathbf{n}$ [12]. Thus, electrostatic interactions disfavor both splay deformations and the tilting of polarization at the surfaces. The role of these interactions in polar ordering remains an intriguing while not fully understood aspect of ferroelectric nematic behavior [15].

Here, we report experimental study on how modifications of surface charges and electrical screening affect polar ordering in ferroelectric nematic liquid crystal RM734. We show that when confined between two glass plates coated with ionic polymers, a stable modulated phase arises within a narrow temperature range between the nematic and ferroelectric nematic phases. Via optical microscopic imaging, we show that this modulated phase corresponds to the theoretically predicted double splay nematic phase. Specifically, the splay deformations alternate in two orthogonal directions oriented 45° with respect to the cell plane, ensuring that both the polarization and the director at the confining surfaces are parallel to the surfaces. As a result, the maximum modulation wavelength is twice the cell thickness. Experiments with various surface treatments show that only cationic polymeric coatings effectively promote the formation of the double splay nematic phase, underscoring the crucial role of the interplay between electrostatic interactions and flexoelectric coupling. We also examine the topological

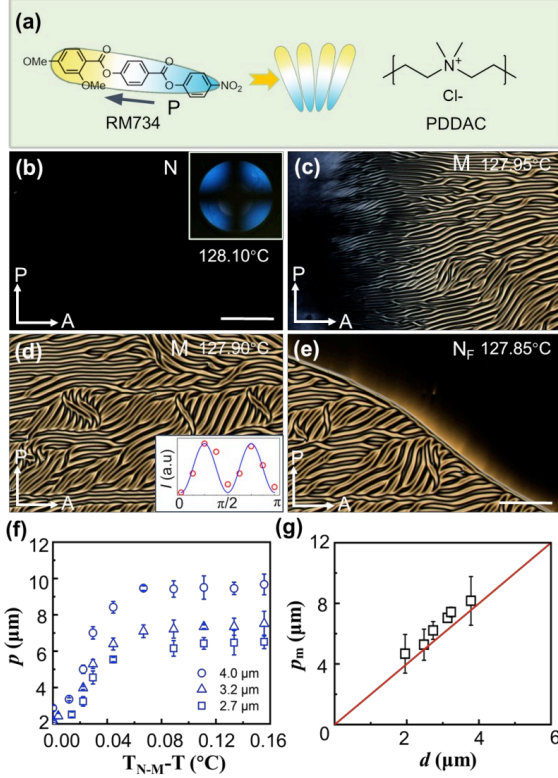


FIG. 1 Materials and the modulated phase. (a) Structures of the RM734 molecule and the cationic polymer PDDAC. (b-e) Polarizing optical microscopic images of the liquid crystal going through the nematic, modulated and ferroelectric nematic phases when temperature is lowered, in a cell of 3.4 μm thickness. The inset in (d) presents measured optical intensity at an arbitrary position versus the orientation angle with the polarizer. (f) Measured modulation wavelength p versus temperature deviation from the onset temperature T_{N-M} . (g) Saturated modulation wavelength p versus cell thickness.

structures within the double splay nematic phase, which display distinct three-dimensional polarization characteristics.

As depicted in Fig. 1a, the RM734 molecule is pear-shaped with an electric dipole moment of ~ 9.8 Debye oriented toward its larger end [3]. The RM734 liquid crystal exhibits well-characterized phases: isotropic (I), nematic (N), ferroelectric nematic (N_F), and crystalline (C), with transition temperatures between them: $T_{I-N}=184^\circ\text{C}$, $T_{N-NX}=132^\circ\text{C}$, $T_{NX-NF}=131^\circ\text{C}$, and $T_{NF-C}=84^\circ\text{C}$, respectively[31].

When the RM734 liquid crystal material is sandwiched between two glass plates with the inner surfaces coated with thin films of cationic polymer PDDAC (poly-diallyldimethylammonium chloride shown in Fig. 1a), a new modulated (M) phase with distinctive optical textures emerges in a narrow temperature between the nematic and ferroelectric nematic phases. When cooled down from $>190^\circ\text{C}$, the liquid crystal undergoes I, N, M, and N_F phases, exhibiting different optical textures under a polarized optical microscope (Figs. 1b-1e). The transition temperatures are as follows: $T_{I-N}=184.0^\circ\text{C}$, $T_{N-M}=128.1^\circ\text{C}$, $T_{M-NF}=127.8^\circ\text{C}$ and $T_{NF-C}=84.0^\circ\text{C}$, respectively.

At $\sim 127.85^\circ\text{C}$, the modulated phase with periodic bright and dark stripe domains emerges from the vertically aligned nematic phase. As the interfaces between them are fuzzy and the modulation wavelength gradually increases away from the interface (Figs. 1c-1d), the transition between them is continuous. At $\sim 127.95^\circ\text{C}$, the N_F liquid crystal emerges from the modulated phase. The transition between M and N_F phases is of first order as evidenced by the sharp interface between them (Fig. 1e).

We measured the modulation wavelengths to investigate temperature effects. To minimize the impact of minor temperature gradients in our hot stage, we focused on the optical textures within a small viewing area ($\sim 20 \mu\text{m}$) at a fixed position. For a given cell thickness, the modulation wavelength (p) initially increases as the temperature decreases, then stabilizes around 0.06°C below the onset temperature T_{N-M} for the modulated phase (Fig. 1f). The saturated or maximal modulation wavelength p_m exhibits a linear dependence on cell thickness (d), which can be fitted by the relationship $p_m = 2d$ (Fig. 1g).

We captured second-harmonic generation (SHG) images of the M and N_F liquid crystals, by using a circularly polarized excitation laser at a wavelength of 800 nm and collecting

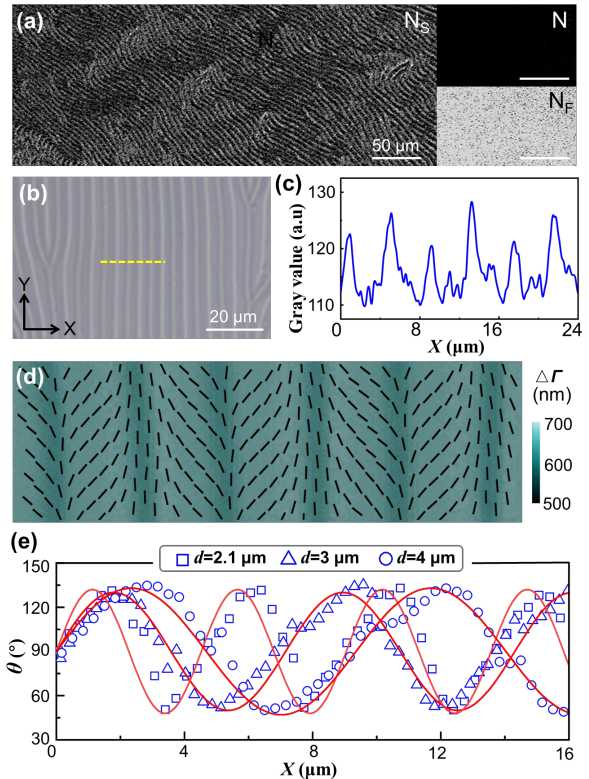


FIG. 2 Polar order and optical microscopic analyses. (a) SHG images of the modulated, the nematic and ferroelectric nematic phases. (b) Bright field optical microscopic image of the modulated phase. (c) Representative intensity profile in the direction perpendicular to the stripes in (b). (d) Measured directors overlaid on the phase retardance. The scale bar is 5 μm . (e) Orientation angles along the X-axis measured at different cell thicknesses. The red lines are fittings with sinusoidal function $\theta(x) = \theta_0 \sin(kX)$.

images at wavelength of 400 nm. The SHG images show periodic intensity modulation in the modulated phase, while uniform intensity in the ferroelectric nematic (N_F) phase (Fig. 2a). Since the SHG effect occurs only in materials with broken inversion symmetry and its intensity is directly proportional to the remnant polarization [33], these observations indicate that the modulated phase exhibits a spatially varying polar order.

We took bright-field optical microscopic images of the modulated phase and found that the stripe domains are separated by parallel bright lines (Fig. 2b). A subtle yet important detail is that these bright lines alternate periodically in their brightness (Fig. 2c).

The modulated phase exhibits no twist in the director across the cell, as the optical intensity under cross-polarized optical imaging can distinguish via sample rotation (inset in Fig. 1d). This allows us to measure the director field $\mathbf{n}(x, y)$ (i.e., the slow optical axis) and the retardance $\Delta\Gamma$ between optical waves polarized along and perpendicularly to the director \mathbf{n} , by using the PolScope technique [34]. The measured director field reveals periodic splay deformations with alternating splay directions while the phase retardance exhibits a small but discernible modulation (Fig. 2d). We can verify that regions with maximal splay correspond to the bright lines observed in the bright-field images.

The orientation angles of the directors relative to the stripe direction (Y axis) exhibit a periodic variation along the perpendicular direction (X axis) (Fig. 2b). This variation can be well fitted by sinusoidal functions, with the fitted amplitudes remaining independent of the cell thickness (Fig. 2e).

This sinusoidal director field appears to be consistent with the single splay nematic phase where the director field is described by: $\mathbf{n}(x) = [\sin\theta(x), 0, \cos\theta(x)]$ with $\theta(x) = \theta_0 \sin(kx)$ [28]. However, this one-dimensional director configuration fails to account for two distinctive features of the M phase: the maximal modulation wavelength being twice of the cell thickness (Fig. 1g) and the alternating brightness of the splay regions under bright-field microscopy (Figs. 2b-2c).

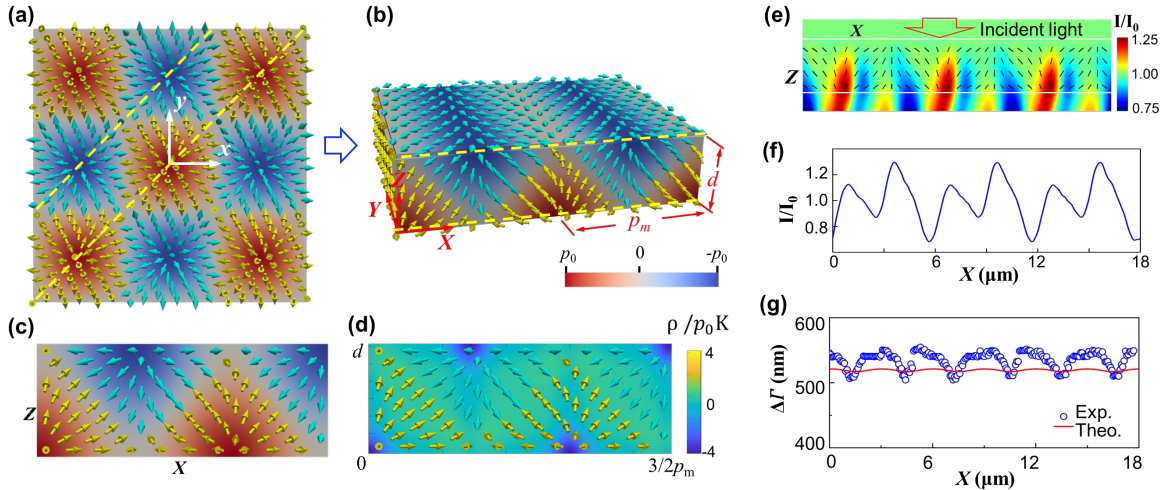


FIG. 3 Structures of double splay nematic phase. (a) Polarization field of the double splay nematic in free space. (b) Polarization field of the double splay nematic confined between two flat surfaces. (c) Polarization field in XZ cross sectional plane. The colors in (a-c) represent the polar order parameter $P_0(x, z)$ as indicated by the scale bar in (b). (d) Distribution of bound charge density in unit of p_0K in XZ plane. (e) FDTD-Calculated optical field distribution in the XZ plane for circularly polarized incident light. (f) Light intensity at the bottom liquid crystal-substrate interface. (g) Calculated retardance (solid red line) compared with experimental data (data points).

These features, however, naturally arise from the double splay nematic phase, as explained below.

The double splay nematic phase is made of two types of domains arranged in a 2D square lattice (Fig. 3a) [21,28]. The polar order parameter $\mathbf{P}(x, y) = P_0(x, y)\mathbf{n}(x, y)$ and the splay vector $\mathbf{n}(\nabla \cdot \mathbf{n})$ align in the same direction within each domain type while point in opposite directions in different domain types (Fig. 3a). The polar order and splay both vanish at the interfaces between these opposing domains [28]. The director \mathbf{n} can be expressed as (Fig. 3a) [28]:

$$\mathbf{n}(x, y) = [\theta_0 \sin kx \cos ky, \theta_0 \cos kx \sin ky, 1]/n_0 \quad (1)$$
where n_0 is a factor to ensure $|\mathbf{n}| = 1$. The amplitude of the polar parameter: $P_0(x, y) \approx 2p_0 \cos kx \cos ky$ [28]. Within the (110) planes defined by $y = x + \pi m/k$ with m being an integer, $n_x = n_y$ and the director is parallel to these planes (dashed lines in Fig. 3a).

Under the confinement of two parallel glass plates, the director (polarization) at the surfaces needs to be parallel to the cell plane to prevent surface charges. The minimal period of the double splay nematic that can satisfy this boundary condition is that bounded by two neighboring (110) planes, as shown by the dash lines in Figs. 3a-3b.

The director field of this configuration in the XYZ coordinates can be obtained by applying a 45° rotation around z -axis followed by a 90° rotation around x -axis, represented by the rotation matrix $R = R_z(\pi/4)R_x(\pi/2)$. The director field can be obtained via $\mathbf{n}(X, Y, Z) = R\mathbf{n}(x, y, z)$ as:

$$\mathbf{n}(X, Z) = [\theta_0 \sin(KX), 1, -\theta_0 \sin(KZ)]/n_0 \quad (2)$$
where $K = k/\sqrt{2}$. The polar order parameter is given by:

$P_0(X, Z) = 2p_0 \cos[K(X - Z)] \cos[K(X + Z)]$. This leads to the maximal modulation wavelength being twice of the cell thickness $p_m = 2d$ (Fig. 3b), and thus $K = 2\pi/p_m = \pi/d$.

Figures 3b-3c illustrates the polar order parameter $\mathbf{P}(X, Z)$ in the XY and ZY planes. Notably, the polarizations at the two confining surfaces are antiparallel. Figure 3d presents the spatial distribution of bound charge density $\rho_B = -\nabla \cdot \mathbf{P}$, in XZ plane and plotted in units of p_0K .

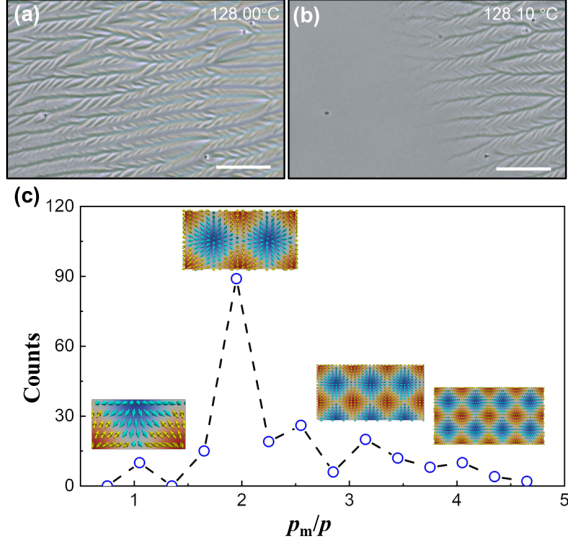


FIG. 4 Transition from the double splay nematic to nematic. (a-b) Representative bright field images of evolving stripe domains upon heating. The scale bars represent 20 μm . (c) Counted numbers of sub-domains at different spatial modulation wavelength (p). The inset images are the polarization fields in the XZ plane corresponding to $p_m/p = 1, 2, 3, 4$.

To gain basic understanding on the bright lines in bright field imaging, we calculated optical field distributions for the confined double splay nematics by employing finite-difference time-domain (FDTD) method to numerically solve the Maxwell equations. The FDTD method has been widely used for calculating optical properties of anisotropic media like liquid crystals[35,36]. The details of calculations are included in the supporting materials.

While the interaction of light with the modulated liquid crystal is complex (Fig. 3f), the calculated intensity profile at the interface between the liquid crystal and substrate is in close resemblance with that observed in the bright field imaging (Fig. 3f and Fig. 2c). The underlying physics is that the alternating triangular domains behave like two small lenses, focusing light into lines, while the top and bottom triangles give rise to uneven light intensity because of different focus. As a contrast, the calculated intensity distribution at liquid crystal interface

for single splay nematics does not exhibit variation in line intensity (see Fig. S1 in SM).

To understand the PolScope results, we look at the director $\mathbf{n}(X, Z)$, which represents the principle optical axis at position (X, Y, Z) . Its polar angle with respect to Z-axis is given as: $\varphi(X, Z) = \arctan \left[\sqrt{1/\theta_0^2 + \sin^2 KX} / \sin KZ \right]$. Its azimuthal angle ϕ with respect to X-axis is: $\phi(X) = \arctan[1/\theta_0 \sin(KX)]$, that is only X dependent, meaning no twist of the director across the cell. For light propagating in the Z-direction, the refractive index is n_o when the polarization is normal to the plane formed by Z-axis and the vector \mathbf{n} , while is: $n_{eff} = (\cos^2 \varphi/n_o^2 + \sin^2 \varphi/n_e^2)^{-1/2}$ for polarization parallel to this plane. The retardance between these two orthogonally polarized optical waves is $\Delta\Gamma = \int_0^d 2\pi(n_{eff} - n_o)dZ$. By taking $n_e=1.71$ and $n_o=1.52$ [37], we numerically calculated $\Delta\Gamma$ for different X and can reproduce the periodic variations observed in PolScope (Fig. 2d). Quantitatively, the variations of the calculated $\Delta\Gamma$ with X is much smaller than the PolScope results (Fig. 3g), due likely to the non-straight propagation of light in the liquid crystal.

Another evidence supporting this confined double splay configuration comes by studying the transition from the double splay nematic to the N phase. When heated at a rate of 0.05°C/min, new stripes with smaller modulation wavelengths emerge within the stripe domains, with a tilt angle between them (Fig. 4a). At ~128.10°C, these sub-stripes smear out to become a homogeneous nematic (N) phase, with a continuous phase boundary (Fig. 4b). We measured the separation (p) between neighboring sub-stripe domains and counted the number of sub-stripe pairs with similar modulation wavelengths (Fig. 4c). The maximal occurrence appears at $p_m/p = 1, 2, 3, 4$. This is consistent with the confined double splay nematic model, namely the newly formed stripe sub-domains consist of diagonal double splay nematic layers bounded by (110) planes, as schematically illustrated in the insets of Fig. 4c.

The RS theory provided mathematical expressions for the parameters, θ_0 , p_0 and k [28]. Near the critical temperature of the N-N_S transition, θ_0 is related to the temperature and elastic constants by: $\theta_0 = 2^{3/2}K_{11}\delta\mu^{1/2}/(3K_{33})^{1/2}\lambda$, where $\mu = \mu(T - T_0)$. Given that $T - T_c$ is less than 0.2 °C, we can estimate that the high order term is negligible. By taking $K_{11} = 1$ pN, $K_{33} = 1$ pN, $\mu = -1 \times 10^3$ Jm/C², $\lambda = 10^{-4}$ V[13], we can estimate that $\theta_0 \sim 60^\circ$, which is reasonably close to the experimental data $\sim 80^\circ$.

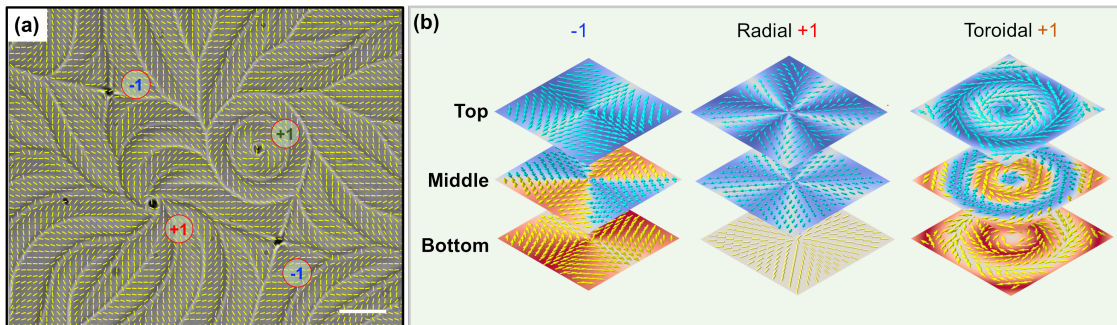


FIG. 5 Topological defects in confined double splay nematics. (a) Exemplary measured director field overlaid on bright field optical image, where -1, toroidal +1 and radial +1 topological defects are indicated. Scale bar is 10 μm . (b) Constructed polarization fields of -1, toroidal +1 and radial +1 topological defects.

The RS theory shows that the modulation wavelength decreases rapidly and reaches a minimum right below the $N-N_s$ transition temperature, and then go up again when the temperature is lowered. We only observed growths of the modulation wavelengths with decreasing temperature (Fig. 1f), that is in good agreement with the second region of the theoretical prediction.

Ionic coatings on the confining surfaces are crucial to the formation of this double splay nematic phase. We tested cationic polymers, anionic polymers and small ionic molecules (see supplemental materials Fig. S2). We observed robust double splay nematic with cationic polymeric dopants, while no modulated phase for anionic polymers. We observed modulated an intermediate phase using small ionic surfactant molecules CTAB, but their structures are complex and remain to be confirmed if it is a double splay nematic. These observations indicate that both the charges and sizes of the dopants significantly influence the formation of the double splay nematic phase[15].

The effectiveness of cationic polymeric coatings in facilitating the double splay nematic order under confinement can be attributed to their ability to address the bound charges at surfaces and in the bulk. With the configuration of double splay nematic under confinement, the bound charges are primarily negative at surfaces while positive in the bulk (Fig. 3d). The cationic polymers coating at the surfaces can neutralize these negative bound charges, while the negatively charged ions dissociated from the polymers are mobile and can effectively compensate for other regions with positive bound charges by reducing the Debye screening lengths. This interaction between the cationic coatings and the bound charges facilitates the stabilization of the double splay nematic phase.

The double splay nematic phase also exhibits intriguing topological defects. There exist three distinct types of topological defects: -1 defect with quartic symmetry, +1 defect with radial splay stripes, and +1 defect with toroidal splay (Fig. 5a). The basic understanding gained about the confined double splay nematic enables us to construct the polarization fields of these defects from optical microscopic measurements.

The -1 defect features a singular defect center where four splay stripes converge (Fig. 5b). Under bright-field optical imaging, these four maximal splay regions alternate in brightness, indicating that they are positioned at opposite surfaces (Fig. S3). The +1 defect with radial splays features five splay stripes radiating outward from the center, with the splay and polarization vectors pointing radially outward (Fig. 5a). These stripes are all located on the same surface, as evidenced by the uniform brightness of the five splay regions under bright field imaging (Fig. 5b). For the +1 defect with toroidal splay, the director field exhibits rotational symmetry. The bright-field image shows that the inner splay region is dimmer than the outer splay region (Fig. 5a), indicating that these two splay regions originate from different confining surfaces. Consequently, the rotation directions of the polarization vectors are opposite at the two surfaces (Fig. 5b).

In conclusion, we have shown that double splay nematic order can be facilitated to form in confined polar fluids by modifying surface charges and electrical screening via cationic polymer coatings, where splay deformations alternate between two orthogonal directions oriented at 45° to the cell plane, aligning both the director and polarization parallel to the cell

surfaces. These findings not only confirm the existence of the theoretically predicted double splay order but also provide fundamental insights into the intricate interplay between electrostatic interactions and flexoelectric effects. These experimental results can inspire more experimental and theoretical studies on how ionic doping affects polar ordering and topological structures, and explorations of new applications in non-linear and quantum optics by taking advantage of the polar order with precisely controllable modulation wavelengths.

We acknowledge the financial support the National Key Research and Development Program of China under grant 2022YFA1405000, the National Natural Science Foundation of China under grants 6210030761 and 12174177, and the Guangdong Basic and Applied Basic Research Foundation under grant 2024B1515040023. We extend our gratitude to J. V. Selinger and R. B. Selinger for their valuable discussions and to Zening Hong for his technical assistance.

*Correspondence to: weiqh@sustech.edu.cn

- [1] P. G. de Gennes, *The Physics of Liquid Crystals* (Clarendon Press, Oxford, 1993), Vol. 2.
- [2] M. Born, *Ueber anisotrope Flüssigkeiten: Versuch einer Theorie der flüssigen Kristalle und des elektrischen Kerr-Effekts in Flüssigkeiten* 1916).
- [3] R. J. Mandle, S. J. Cowling, and J. W. Goodby, *Phys. Chem. Chem. Phys.* **19**, 11429 (2017).
- [4] H. Nishikawa, K. Shiroshita, H. Higuchi, Y. Okumura, Y. Haseba, S. I. Yamamoto, K. Sago, and H. Kikuchi, *Adv. Mater.* **29**, 1702354 (2017).
- [5] X. Chen *et al.*, *Proc. Natl. Acad. Sci. U.S.A.* **117**, 14021 (2020).
- [6] O. D. Lavrentovich, *Proc. Natl. Acad. Sci. U.S.A.* **117**, 14629 (2020).
- [7] N. Sebastián, M. Čopič, and A. Mertelj, *Phys. Rev. E* **106**, 021001 (2022).
- [8] A. Erkoreka, N. Sebastián, A. Mertelj, and J. Martinez-Perdiguero, *J. Mol. Liq.* **407**, 125188 (2024).
- [9] P. Kumari, B. Basnet, M. O. Lavrentovich, and O. D. Lavrentovich, *Science* **383**, 1364 (2024).
- [10] B. Basnet, M. Rajabi, H. Wang, P. Kumari, K. Thapa, S. Paul, M. O. Lavrentovich, and O. D. Lavrentovich, *Nat. Comm.* **13**, 3932 (2022).
- [11] J. Yang, Y. Zou, W. Tang, J. Li, M. Huang, and S. Aya, *Nat. Comm.* **13**, 7806 (2022).
- [12] P. Kumari, B. Basnet, H. Wang, and O. D. Lavrentovich, *Nat. Comm.* **14**, 748 (2023).
- [13] J. Yang, Y. Zou, J. Li, M. Huang, and S. Aya, *Nat. Phys.* **20**, 991 (2024).
- [14] Y. Zou, J. Yang, X. Zhang, M. Huang, and S. Aya, *Soft Matter* **20**, 3392 (2024).
- [15] Z. Ma *et al.*, arXiv preprint arXiv:2406.00994 (2024).
- [16] S. Yi *et al.*, arXiv preprint arXiv:2406.13326 (2024).
- [17] J. Karcz, J. Herman, N. Rychłowicz, P. Kula, E. Górecka, J. Szydłowska, P. W. Majewski, and D. Pocięcha, *Science* **384**, 1096 (2024).
- [18] C. J. Gibb *et al.*, *Nat. Comm.* **15**, 5845 (2024).
- [19] H. Nishikawa, D. Okada, D. Kwaria, A. Nihonyanagi, M. Kuwayama, M. Hoshino, and F. Araoka, *Adv. Sci.* **11**, 2405718 (2024).
- [20] R. B. Meyer, *Phys. Rev. Lett.* **22**, 918 (1969).
- [21] J. V. Selinger, *Annu. Rev. Condens. Ma. P.* **13**, 49 (2022).

- [22] S. Dhakal and J. V. Selinger, Phys. Rev. E **81**, 031704 (2010).
- [23] R. J. Mandle, N. Sebastián, J. Martinez-Perdiguero, and A. Mertelj, Nat. Comm. **12**, 4962 (2021).
- [24] L. Paik and J. V. Selinger, arXiv preprint arXiv:2408.10347 (2024).
- [25] Y. Zou and S. Aya, Phys. Chem. Chem. Phys. **26**, 15637 (2024).
- [26] J. V. Selinger, Liq. Cryst. Rev. **6**, 129 (2018).
- [27] M. Čopič and A. Mertelj, Phys. Rev. E **101**, 022704 (2020).
- [28] M. P. Rosseto and J. V. Selinger, Phys. Rev. E **101**, 052707 (2020).
- [29] A. Mertelj, L. Cmok, N. Sebastián, R. J. Mandle, R. R. Parker, A. C. Whitwood, J. W. Goodby, and M. Čopič, Phys. Rev. X **8**, 041025 (2018).
- [30] N. Sebastián, L. Cmok, R. J. Mandle, M. R. de la Fuente, I. D. Olenik, M. Čopič, and A. Mertelj, Phys. Rev. Lett. **124**, 037801 (2020).
- [31] J. Thoen, G. Cordoyiannis, E. Korblova, D. M. Walba, N. A. Clark, W. Jiang, G. H. Mehl, and C. Glorieux, Phys. Rev. E **110**, 014703 (2024).
- [32] P. Nacke *et al.*, Sci. Rep. **14**, 4473 (2024).
- [33] P. Franken and J. F. Ward, Rev. Mod. Phys. **35**, 23 (1963).
- [34] M. Shribak and R. Oldenbourg, Appl. Optics **42**, 3009 (2003).
- [35] C. Oh and M. J. Escuti, Opt. Express **14**, 11870 (2006).
- [36] S. Liu, H. Yu, M. Jiang, L.-L. Ma, Y.-Q. Lu, and Q.-H. Wei, Phys. Rev. Mater. **8**, 085201 (2024).
- [37] N. Sebastián *et al.*, Nat. Comm. **14**, 3029 (2023).